Organometallics as Therapeutic Agents

Contents

1. Introduction

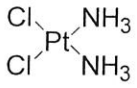

cisplatin

*landmark discovery
*severe side-effect
*resistance

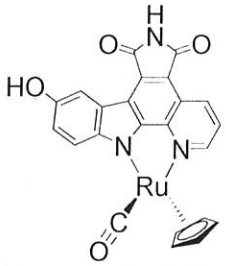

DW 1

*metal as scaffold
*studied by Meggers *et al.*
*protein kinase inhibitor

see Dr. Shibuguchi's lit. sem. 070221

A variety of organometallics as therapeutic agents have been developed recently.

* DNA binder with covalent bond
* DNA binder with non-covalent bond
* metal as scaffold
* protein binder

For a review of organometallics as therapeutic agents, see:
Bruijnincx, P. and Sadler, P. J. *Curr. Opin. Chem. Biol.* **2008**, *12*, 197.

2. G-quadruplex binder

For a general review on G-quadruplex, see: *ChemMedChem* **2008**, *3*, 690.

*Guanine-rich stretches of DNA have a high propensity to self-associate into planar guanine quartets (Figure 1, G-tetrad), and the quartet stacks each other to form G-quadruplex.
*Important roles in some biological events. (telomere, promoter region, ribosomal DNA)
*structural diversity and polymorphism (by nature of loop)

ex. telomere
*Tandem repeat of TTAGGG (human, 5-8kb) and single-stranded overhang of 100-200 bases.
*Telomere becomes shorter after each cell division, and it leads to cellular senescence.
*Normal cell : weak telomerase activity
Cancer cell : high telomerase activity
*Formation and stabilization of G-quadruplex often lead to telomerase inhibition.
*Potential agents for anti-cancer drug.

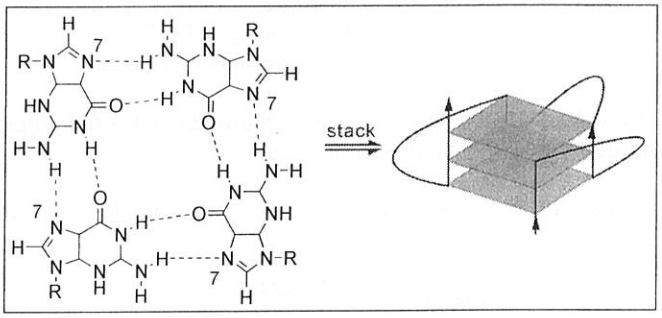

Figure 1. Structure of G-quadruplex

J|A|C|S ARTICLES

J. Am. Chem. Soc. **2009**, *131*, 1835.

Platinum(II) Complexes with Dipyridophenazine Ligands as Human Telomerase Inhibitors and Luminescent Probes for G-Quadruplex DNA

Dik-Lung Ma, Chi-Ming Che,* and Siu-Cheong Yan

Department of Chemistry and Open Laboratory of Chemical Biology of the Institute of Molecular Technology for Drug Discovery and Synthesis, The University of Hong Kong, Pokfulam Road, Hong Kong

2.1. Motivation and synthesis

Planar π-conjugated molecule is known to bind to and stabilize G-quadruplex.
Platinum(II) complexes containing aromatic diimine ligands are known to have rich photoluminescent properties.

⇨ Development of photoluminescent telomerase inhibitor ?

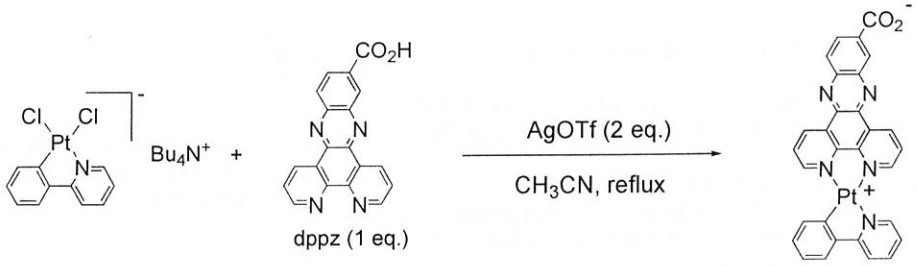

1

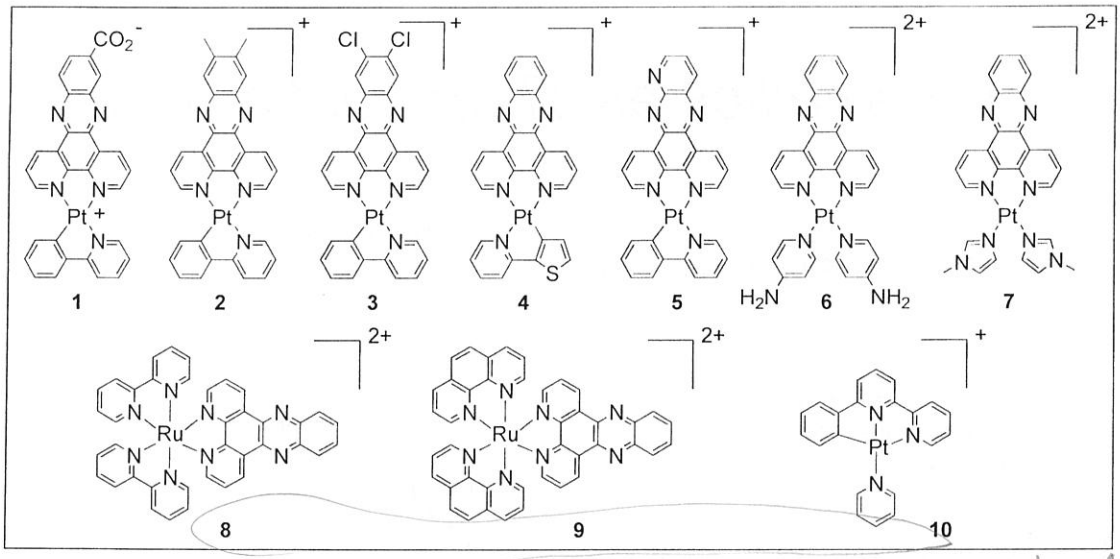

Figure 2. Examined complexes **1** - **10**

These complexes were characterized with ^{1}H NMR, UV-vis, MS, and elemental analysis.

✓ G-quadruplex Binding

2.2. Gel Mobility Shift Assay

*Possible G-quadruplex structure is shown in Figure 3.
*No formation of G-quadruplex without Pt(II) complex (Figure 4, left)
*Pt(II) complex **1** - **7** induced formation of G-quadruplex from TR2 oligonucleotide (Figure 4, left).

Control experiments (data not shown)
*G-quadruplex formation was not observed with oligonucleotide MTR2 [5'-TACAGATAGTTAGACTTAACGTTA-3']
*dppz (3 - 24 μM) didn't induce G-quadruplex formation.

*Use of Telo21 which generates well-characterized G-quadruplex afforded the same result (Figure 4, right).

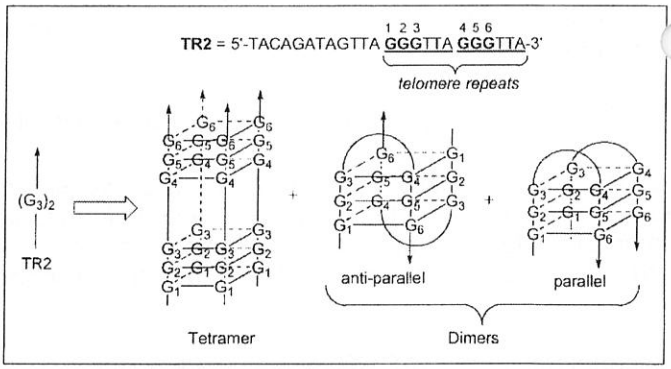

Figure 3. Sequences of oligonucleotide TR2 and possible structures of intermolecular quadruplex.

*Complex **1** has the highest activity. 30% G-quadruplex at 0.6 μM (Figure 5).

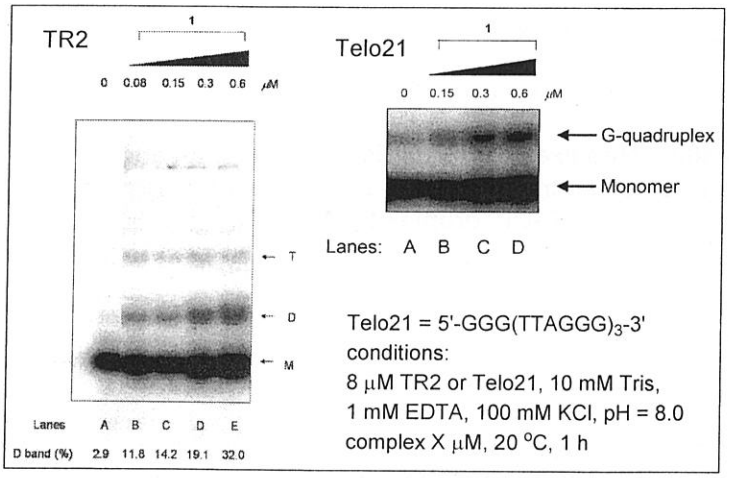

Figure 4. PAGE analysis with TR2 and Telo21 (D:Dimer, T:Tetramer)

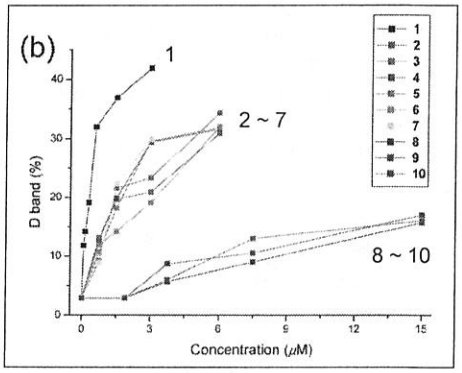

Figure 5. Intensity of band D vs conc.

2.3. Absorption Titration

*Used DNA oligomer is G4A1, which is known to form intramolecular G-quadruplex (Figure 6).
*Addition of G4A1-quadruplex to the aqueous solution of complexes led to 5 nm red shift and 30% hypochromism of the band at 362 nm (Figure 7).

*After pretreatment of the G-quadruplex with dimethyl sulfate (which leads to methylation of N7 position of guanine, essential position for G-quadruplex assembly), same titration experiment was undertaken. No significant spectral changes were observed.

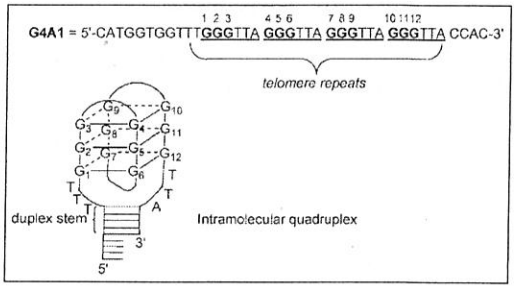

Figure 6. Sequences of oligonucleotide G4A1 and possible structure of the intramolecular quadruplex.

⇨ Spectral changes are NOT attributed to the binding of **1** to the unstructured form of the G_4A_1 oligonucleotide.

A possibility that double-stranded stem region in G4A1-quadruplex DNA interacts with Pt(II) complex cannot be excluded (Figure 6).

⇩

Shorter oligonucleotide G4A2, which has no duplex stem and is known to assemble into an intramolecular G-quadruplex afforded a similar spectral changes (Figure 8).

⇩

Pt(II) complex **1** indeed interacts with G-quadruplex region.

Binding constant was calculated by absorption titration assay.

$$D/\Delta_{\varepsilon ap} = D/\Delta\varepsilon + 1/[(\Delta\varepsilon)K]$$

D is the concentration of DNA

$\Delta\varepsilon_{ap} = |\varepsilon_A - \varepsilon_F|$, $\varepsilon_A = A_{obs}/[complex]$

$\Delta\varepsilon = |\varepsilon_B - \varepsilon_F|$

ε_B and ε_F correspond to the extinction coefficiencients of the DNA-complex adduct and unbound complex, respectively.

ref. *J. Am. Chem. Soc.* **1993**, *115*, 8547.

Table 1. Summary of DNA-binding data for **1** - **10**.

Complex	K at 20 °C/dm^3 mol^{-1}	
	G4A1-quadruplex	Double-stranded DNA[a]
1	$9.7 \pm 1.1 \times 10^6$	$1.2 \pm 0.2 \times 10^4$
2	$6.3 \pm 0.6 \times 10^6$	$2.3 \pm 0.5 \times 10^4$
3	n.d.[b]	n.d.[b]] due to low solubility of complexes
4	n.d.[b]	n.d.[b]
5	$6.1 \pm 1.7 \times 10^6$	$1.9 \pm 0.2 \times 10^4$
6	$6.6 \pm 0.8 \times 10^6$	$1.1 \pm 0.1 \times 10^4$
7	$1.9 \pm 0.3 \times 10^6$	$1.2 \pm 0.1 \times 10^4$
8	$5.8 \pm 0.6 \times 10^4$	$3.3 \pm 0.4 \times 10^4$
9	$6.3 \pm 0.3 \times 10^4$	$3.6 \pm 0.3 \times 10^4$
10	$2.0 \pm 0.9 \times 10^4$	$2.5 \pm 0.3 \times 10^4$

[a] Non-quadruplex double-stranded DNA molecules consisting of complementary G4A1 oligos. [b] Not determined.

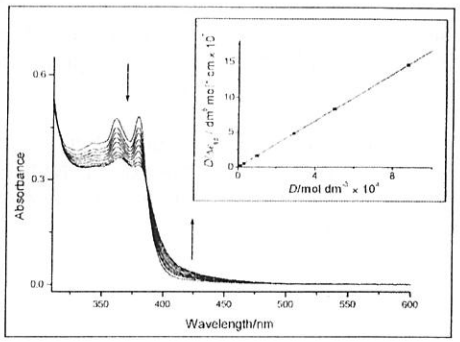

Figure 7. UV-vis spectra of **1** with increasing amounts of G4A1 ([G-quadruplex] / [Pt] = 0 - 20).

conditions: [Pt] = 50 μM, 10 mM Tris HCl, 100 mM KCl pH = 7.5, [G-quadruplex] = 0 - 1000 μM

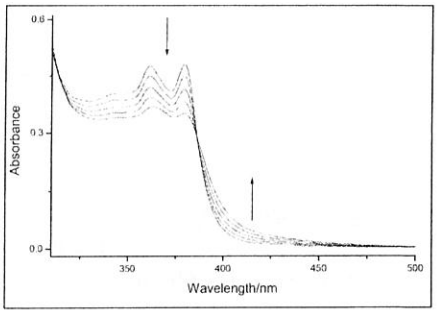

Figure 8. UV-vis spectra of **1** with increasing amounts of G4A2 ([G-quadruplex] / [Pt] = 0 - 20).

conditions: [Pt] = 50 μM, 10 mM Tris HCl, 100 mM KCl pH = 7.5, [G-quadruplex] = 0 - 1000 μM

G4A2 : [5'-AGGG(TTAGGG)$_3$-3']

The highest affinity and selectivity was exhibited by **1**.
(~ 800-fold compared to double-stranded DNA binding)
(Representative binder, BRACO19 shows 25-fold difference.)

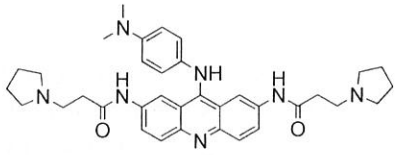

BRACO19

ref. Neidle, S. et al. *J. Med. Chem.* **2003**, *46*, 4463.

2.3. UV Melting Study

Upon treatment of the G4A1-quadruplex (20 μM) with an equimolar amount of **1**, a marked increase in T_m (DNA melting temperature, ΔT_m = 14 °C) was registered.

Complex **1** induces (Figure 4), binds to (Figure 7, 8), and stabilizes (Section 2.3.) G-quadruplex.

✓ Photoluminescent Nature of Complex **1**

2.4. Emission Titration & Detection of G-quadruplex in PAGE

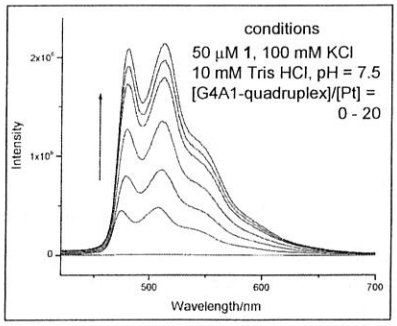

Figure 9. Emission spectral traces of **1**

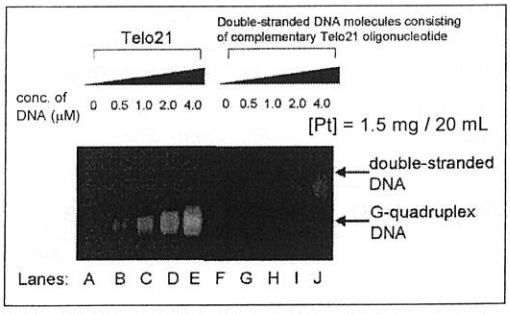

Figure 10. Emissive PAGE analysis

Emission at 512 nm reached 293-fold increase with 20-fold amount of complex **1** (Figure 9).
Double-stranded G4A1 and G4A1 pretreated with dimethyl sulfate didn't significantly increase the emission intensity (data not shown).

Pt(II) complex **1** can be used as stain (Figure 10).

✓ Binding Mode

2.5. NMR experiments

*Addition of **1** caused a significant peak broadening and a large change in the chemical shift of the imino protons of G-quadruplex (Figure 11).
*Broadening might be due to an exchange at intermediate rate on the NMR time scale between bound and non-bound states.

*G5 imino proton showed the largest shift.
(Assignment of proton was based on 2D NMR and precedent literatures.)
*Authors expected external end-binding mode rather than intercalating mode between G-tetrads (Figure 12).

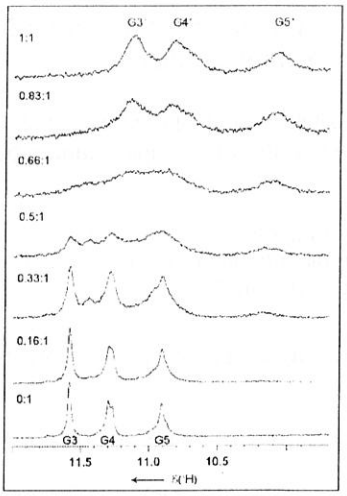

Figure 11. NMR titration of G4A3-quadruplex with **1** in 90% H_2O / 10% D_2O, 27 °C
Only the imino proton signals are shown.
G4A3 (5'-TAGGGTTA-3')

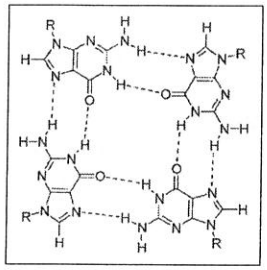

G-tetrad

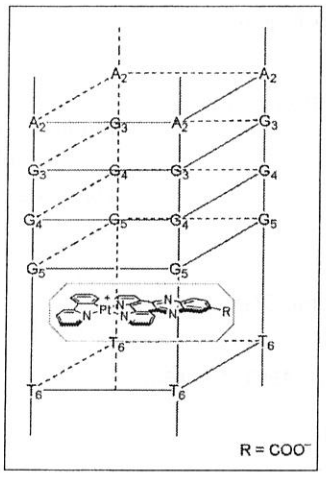

Figure 12. Plausible binding mode

2.6. Molecular Modeling

Table 2. Calculated binding energy

G-quadruplex-1	Binding energy (kcal/mol)			
	end stacking at 3′ (1)[a]	intercalation near 3′ (2)[a]	intercalation near 5′ (3)[a]	end stacking at 5′ (4)[a]
$d(T_2AG_3T)_4$–1	−54.00	20.60	20.80	−35.34

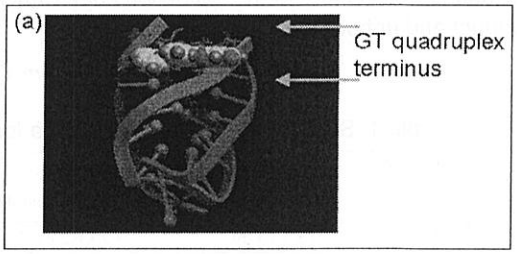

Figure 13. Molecular modeling of the binding interaction between **1** and intermolecular four stranded G-quadruplex DNA ($(T_2AG_3T)_4$)

*External end-binding mode was preferential compared to intercalation (Table 2 & Figure 13).

2.7. Telomerase Inhibition Assay

*A 5'-biotinylated primer consisting of three telomeric repeats was used, and the incorporation of ^{32}P-labeled GTP was measured.

*$^{tel}IC_{50}$ = 760 nM
(Many other inhibitors show IC_{50} values of 100 - 500 nM)
*Other experiments determined IC_{50} value to cancer cells (17 - 25 μM)
*IC_{50} value to normal cell (180 μM) : ~ 10 times less cytotoxic.

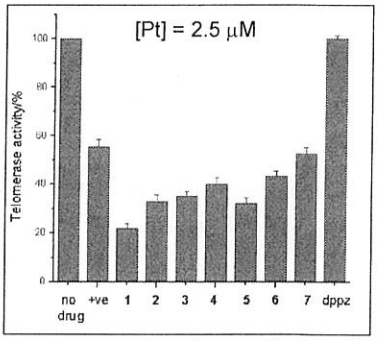

Figure 14. Cell-free inhibition of telomerase

2.8. Other (Organometallics-based) G-quadruplex Binders

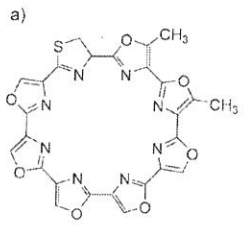

telomestatin
$^{tel}IC_{50}$ = 5 nM
(strongest)

Shin-ya, K. and Seto, H et al.
J. Am. Chem. Soc.
2001, *123*, 1262.

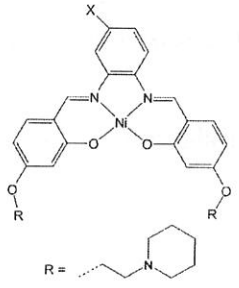

$^{tel}IC_{50}$ = 120 - 140 nM

Neidle, S. and Vilar, R. et al.
J. Am. Chem. Soc.
2002, *124*, 2098.

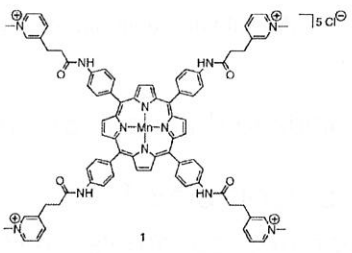

$^{tel}IC_{50}$ = 580 nM
10000-fold selectivity between G-quadruplex and duplex DNA

Pratviel, G. et al.
J. Am. Chem. Soc.
2007, *129*, 1502.

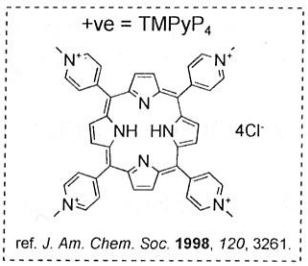

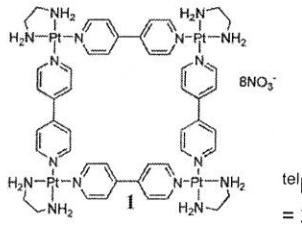

$^{tel}IC_{50}$ = 200 nM

Autexier, C., Moitessier, N., Sleiman, H. F. et al.
J. Am. Chem. Soc. **2008**, *130*, 10040.

Appropriate size, extended π–conjugation, and cationic nature.

2.9. Outlook

Selectivity among G-quadruplexes should be important because human genes contain as many as 376,000 quadruplex-forming sequences.

3. Catalytic Drugs (Co^{III}-cyc : artificial protease)

For a review, see: Suh, J. and Chei, W. S. *Curr. Opin. Chem. Biol.* **2008**, *12*, 207.

*Dosage can be reduced, which would lead to less side-effect.
*Strong binding to the target is not required if the peptide cleavage is fast enough.
*Drug for the proteins lacking active sites can be developed.

The 1st example of synthetic metal catalyst for hydrolytic cleavage of intact protein even in a non-selective manner.

Burstyn, J. N. et al *J. Am. Chem. Soc.* **1995**, *117*, 7015.

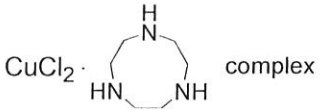

BIOORGANIC & MEDICINAL CHEMISTRY

Toward Protein-Cleaving Catalytic Drugs: Artificial Protease Selective for Myoglobin

Joong Won Jeon, Sang Jun Son, Chang Eun Yoo, In Seok Hong and Junghun Suh*
School of Chemistry and Center for Molecular Catalysis, Seoul National University, Seoul 151-747, South Korea

Communication : *Org. Lett.* **2002**, *4*, 4155.
Full paper : *Bioorg. Med. Chem.* **2003**, *11*, 2901.

3.1. Approach and Synthesis

*Catalyst site and binding site was connected via amide bond (Figure 1).
*Cyc-Metal complex was used as catalytic sites.
*PNA (peptide nucleic acid) was used as binding sites.

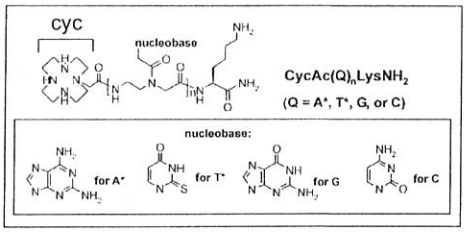

Figure 1. Structure of CycAc(Q)$_n$Lys-NH_2

*Combinatorial approach was used for the search of active catalyst. (Split-Pool method)
*The library of CycAc(Q)$_n$LysNH_2 (total 75 μM) was mixed with $CuCl_2$ aq (350 μM) to generate the library of Cu(II)CycAc(Q)$_n$LysNH_2.

*The library containing 7- or 8-mer PNAs showed no activities (checked with PAGE).
*The library containing 9-mer PNA showed cleavage activity toward Mb.
*After minute study of the library (PNA sequences and ligand of Cu), **1** was chosen as the best (Figure 2).

A* recognizes T, and T* recognizes A. However, A* and T* do not recognize each other.

⇩

prevention of base-pairing among PNA mixtures present in the library.

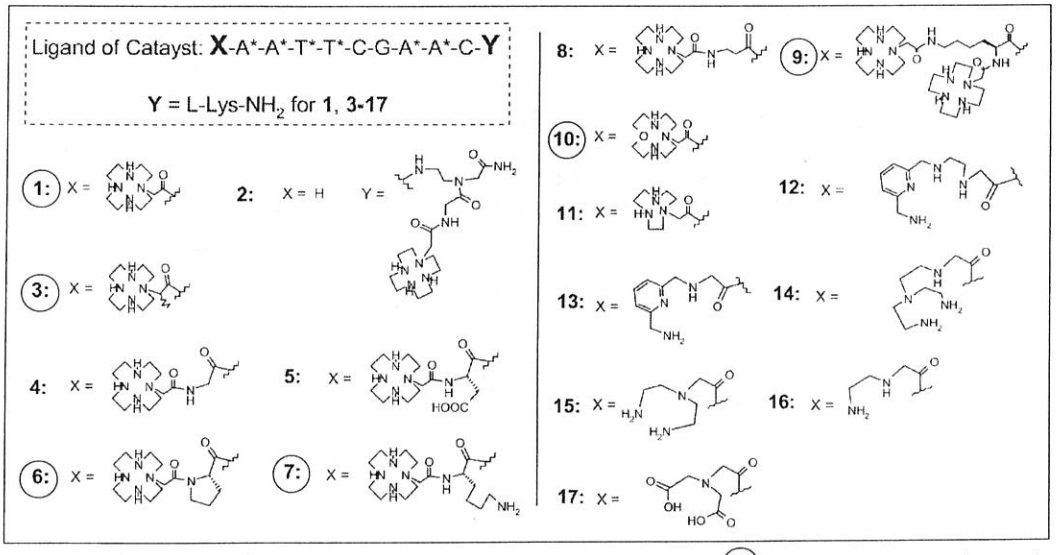

Figure 2. Structures of **1** - **17**

◯ : Mb cleavage was observed

*2 : C-terminal Lys is important? or catalytic center is not located in a productive position in the Co(III)**2**-Mb complex?
*4, 5, 8 : Elongation of linker was not good probably due to too much rotational freedom of acetyl moiety, which reduced the effective molarity of catalytic center in the catalyst-Mb complex.
*6, 7 : Proline (**6**) manifested the catalyst activity perhaps due to its unique conformation.
Lysine (**7**) also manifested the catalyst activity probably due to productive conformation provided by electrostatic interaction between ε-amino group and Mb surface??
*11 - 17 : Ligands other than Cyclene were bad.

*Complex formation

$CuCl_2$ aq. + **1 - 17** $\xrightarrow[pH = 6.0]{}$ complex
1 eq. 1.2 eq.

$CoCl_2$ aq. + **1 - 17** $\xrightarrow[MeOH]{LiOH}$ Co(II) complex $\xrightarrow[MeOH]{air}$ Co(III) complex
1 eq. 1.2 eq.

due to inert ligand exchange of Co(III)

Catalysts were characterized with UV-vis (appearance of λ_{max} around 510 nm) and MALDI-TOF-MS.

3.2. Kinetics of Mb Cleavage

*Decrease of [Mb] was calculated with SDS-PAGE (Figure 3).
*Pseudo-1st-order kinetics

$$k_o\ (Cu) = 5.7 \times 10^{-3}\ h^{-1}, \qquad k_o(Co) = 9.4 \times 10^{-3}\ h^{-1}$$

*Co shows higher reactivity than Cu.
*Up to 6 molecules of Mb were cleaved by each molecule of Co(III)**1**.
*Subsequent experiments were performed with Co(III) complex.

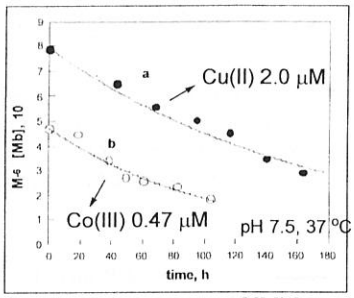

Figure 3. Decrease of [Mb]

*k_o was measured with a variety of initial catalyst concentration (C_o) (Figure 4).
*When C_o < $[Mb]_o$, linear increase of k_o.
When C_o > $[Mb]_o$, constant k_o value.
This observation agrees with strong binding of Mb to Co(III)**1**.
*k_o measured with C_o greater than $[Mb]_o$ corresponds to k_{cat} (Table 1).

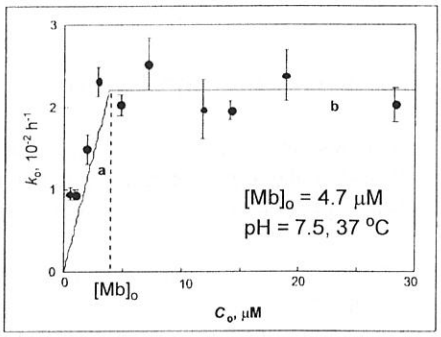

Figure 4. k_o against C_o by Co(III)**1**

*Bell-shaped pH profile was obtained (Figure 5).
It is noteworthy that the catalyst is most active at the physiological pH.

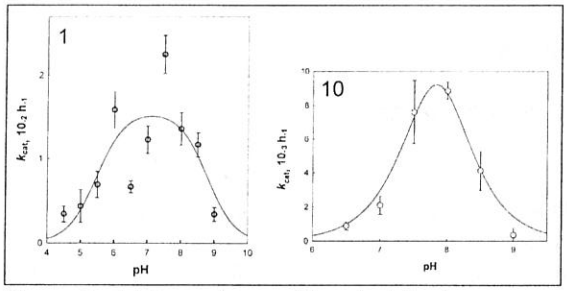

Figure 5. pH dependence of k_{cat} for Mb cleavage by Co(III)**1** and Co(III)**10**

Table 1. Values of k_{cat} measured at optimum pH and 37 °C for the Co(III) complexes of **1**, **3**, **6**, **7**, **9**, and **10**

Catalyst	k_{cat} (10^{-3} h^{-1})[a]	Optimum pH
Co(III)**1**	22	7.5
Co(III)**3**[b]	2.8	7.5
Co(III)**6**	2.4	7.5
Co(III)**7**	2.4	7.5
Co(III)**9**	4.4	7.5
Co(III)**10**	8.9	8.0

[a]Relative standard deviation: 10–20%.
[b]For the two enantiomers of **3X**, only one may lead to an active artificial protease. Thus, the observed k_{cat} value may underestimate the actual catalytic capability.

3.3. Characterization of cleavage site

*Co(III)**1** dissected Mb into two pairs of proteins, which are difficult to be separated by PAGE (Figure 6 left, Table 2).
*Co(III)**3**, **6**, **7**, **9** afforded single pair of fragments (Figure 6 right, Table 2).
*Product solution by Co(III)**3** was subject to *N*-terminal sequencing by Edman degradation.

⇩

Leu_{89}-Ala_{90} is the cleavage site and success of Edman degradation supports the hydrolytic nature of cleavage.

Table 2. Molecular weights of protein fragments disclosed by MALDI-TOF MS and cleavage sites proposed to account for the protein fragments

Catalyst	*m/z* of fragments	Cleavage site proposed on the basis of *m/z* values[a]
Co(III)**1**	7074, 9891, 8045, 8909	Leu_{89}-Ala_{90}, Leu_{72}-Gly_{73}
Co(III)**3**	7066, 9897	Leu_{89}-Ala_{90}
Co(III)**6**	7066, 9898	Leu_{89}-Ala_{90}
Co(III)**7**	7068, 9888	Leu_{89}-Ala_{90}
Co(III)**9**	7068, 9884	Leu_{89}-Ala_{90}
Co(III)**10**	7075, 9896	Leu_{89}-Ala_{90}

[a]M_r of protein fragments to be obtained: 7059 and 9893 for cleavage at Leu_{89}-Ala_{90}, 8056 and 8896 for cleavage at Leu_{72}-Gly_{73}.

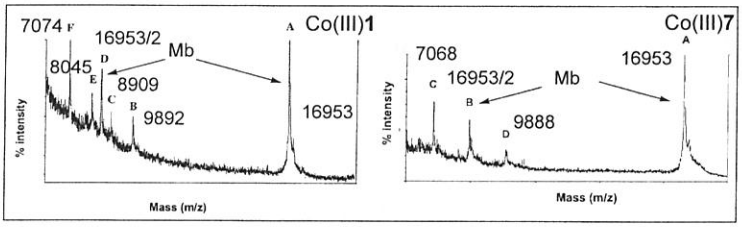

Figure 6. MALDI-TOF-MS taken after incubation of Mb with Co(III)**1** and Co(III)**7**
left : Co(III)**1** (3.5 μM), Mb (12 μM), pH = 6.0, 37 °C, 85 h
right : Co(III)**7** (9.8 μM), Mb (9.8 μM), pH = 7.5, 37 °C, 96 h

*So far, it is not clear whether the two cleavage sites involve different Co(III)**1**-Mb complexes or originate from an identical one.

3.4. Control Experiments

*Fe(III), Hf(IV), Pt(IV), Zr(IV), Pd(II), or Ce(IV) complex didn't cleave Mb.
*Other proteins such as albumin, γ-globulin, elongation factor P, gelatin A, and gelatin B were not cleaved by Cu(II)**1** or Co(III)**1**.
*Neither $CuCl_2$, Cu(II)Cyc, nor Co(III)Cyc cleaved Mb.
*Cu(II)**18** and Co(III)**18** have no catalytic activities (For **18**, see below).
*Amide bonds in the catalyst were not cleaved under the conditions of kinetic measurements (checked with MALDI-TOF MS).
*Removal of O_2 didn't affect the rate of cleavage of Mb (which supports non-oxidative peptide cleavage).

1 = CycAc-A*-A*-T*-T*-C-G-A*-A*-C-$LysNH_2$
18 = CycAc-C-A*-T*-T*-C-G-A*-A*-C-$LysNH_2$

3.5. Plausible Mechanism (Figure 7)

*NaOH titration of related [Co(oxacyclen)CO_3](ClO_4) complex indicated the presence of two aqua ligands under aqueous conditions, which suggests the catalytic species as A form.
*Co(III) acts as a Lewis acid to enhance the electrophilicity of carbonyl carbon (B).
*Metal-bound hydroxide ion can act as a nucleophile (B to C).
*Expulsion of protonated amine group (C to D).

*The bell-shaped pH profiles of k_{cat} illustrated in Figure 5 agree with the mechanism? Protonation of the hydroxo(B) or oxo (C) ligand at low pH and deprotonation of the ammonium ion (C) at high pH would reduce the reactivity.

*Figure 8 provides information of the stability of the tetrahedral intermediate (C) in the mechanism.

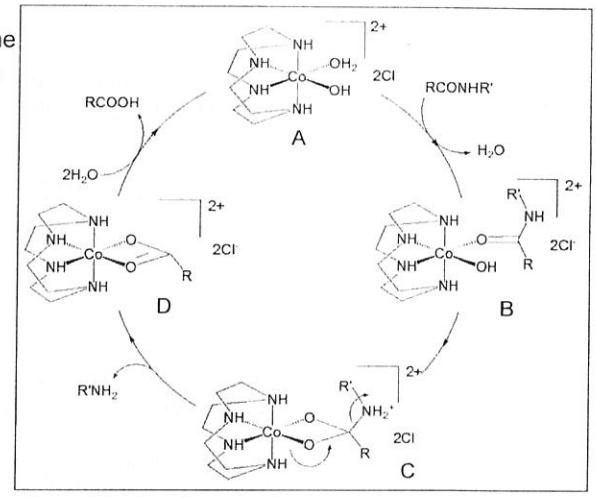

Figure 7. Plausible mechanism

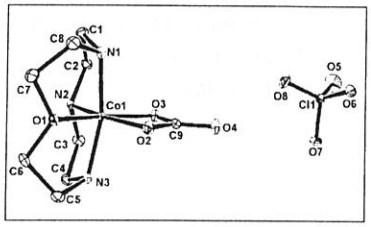

Suh, J. et al
J. Biol. Inorg. Chem. **2009**, *14*, 151.

Figure 8. [Co(oxacyclen)CO_3](ClO_4)

3.6. Other Reports

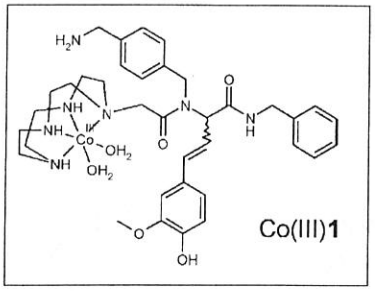

peptidedeformylase-cleaving catalyst.

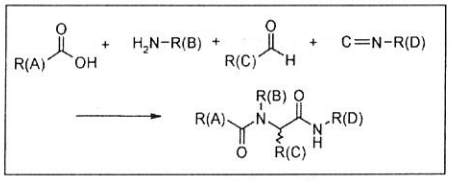

with a library of catalyst candidates synthesized by the Ugi reaction

Suh, J. et al.
J. Am. Chem. Soc. **2005**, *127*, 2396.

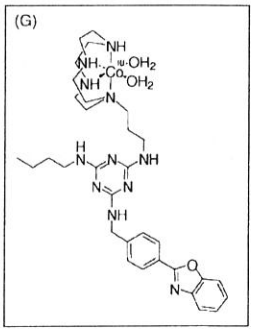

soluble oligomer of Amyloid β peptides-cleaving catalyst

Suh, J. et al.
Angew. Chem. Int. Ed. **2007**, *46*, 7064.

3.7. Outlook

* Higher activity

* in vitro (cell level) and in vivo application

4. Catalytic Drugs (Ru-arene complex)

For a focus review of Ru-arene complex by Sadler, P. J., see:
Peacock, A. F. A. and Sadler, P. J. *Chem. Asian. J.* **2008**, *3*, 1890.

Many of catalytic drugs are peptide-cleaving agents (hydrolytic or oxidative). Here, a different kind of catalytic drugs is shown, which involves generation of reactive oxygen species in cell by catalytic redox reactions.

PNAS

Catalytic organometallic anticancer complexes

Sarah J. Dougan[†], Abraha Habtemariam[‡], Sarah E. McHale[‡], Simon Parsons[‡], and Peter J. Sadler[‡§]

[‡]School of Chemistry, University of Edinburgh, West Mains Road, Edinburgh EH9 3JJ, United Kingdom; and [†]Department of Chemistry, University of Warwick, Gibbet Hill Road, Coventry CV4 7AL, United Kingdom

Proc. Natl. Acad. Sci. USA **2008**, *105*, 11628.

Many metal complexes containing metal-halide bonds are known as anticancer agents.
They are activated in cells by hydrolysis and bind to DNA as a target. *ex.* cisplatin, $[(\eta^6\text{-arene})Ru(en)Cl]PF_6$

$[(\eta^6\text{-biphenyl})Ru(en)Cl]PF_6$ —hydrolysis→ $[(\eta^6\text{-biphenyl})Ru(en)(\underline{OH_2})]Cl(PF_6)$ —DNA→ Guanine-adduct

- 100 mM NaCl aq. (close to extracellular conditions) → Hydrolysis was largely suppressed. (81% intact in 10 mM complex) (> 99% intact in 0.2 mM complex)
- $[(\eta^6\text{-biphenyl})Ru(en)(\underline{OH_2})]Cl(PF_6)$ analyzed by LC-MS (pK_a value of OH_2 was 7.7.) (76% in the case of 2 mM complex)
- Guanine-adduct analyzed by HPLC, ESI-MS, 5'-exonuclease analysis, and ^{1}H-NMR

IC_{50} against A2780 human ovarian cancer cells: 5 μM

ref. Sadler, P. J. et al. *J. Med. Chem.* **2001**, *44*, 3616.
Proc. Natl. Acad. Sci. USA **2005**, *102*, 18269.

In contrast, complexes in this article have different mode of action.

4.1. Synthesis and Structures

$[(\eta^6\text{-p-cymene})RuCl_2]_2$ —KI→ $[(\eta^6\text{-p-cymene})RuI_2]_2$ (y. 86%) —azpy-NMe_2; $NaPF_6$→ $[(\eta^6\text{-p-cymene})Ru(azpy\text{-}NMe_2)I]PF_6$ **1** (y. 68%)

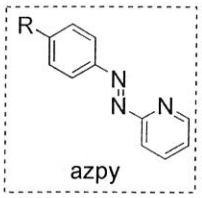

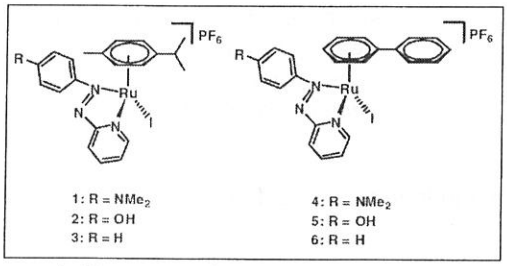

Figure 1. Structures of complexes synthesized in this work.

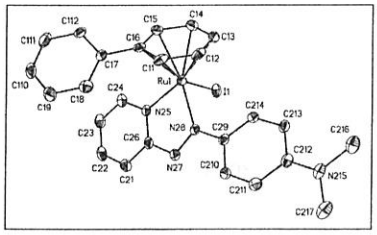

Figure 2. X-ray structure of the cation in 4·MeOH

4.2. Cytotoxicity

*A2780 human ovarian and A549 human lung cancer cell lines were examined (Table 1).
*Complexes **1**, **2**, **4**, and **5** containing electron-donating groups on azpy ligand have IC_{50} values of 2 - 6 μM.
*Complexes **3** and **6** having non-substituted azpy were much less cytotoxic.
*Corresponding chlorido complex afforded dramatic decrease in cytotoxicity. (See remarks in the next page.)
*Azpy ligand alone was relatively nontoxic (except for Azpy-NMe_2 in A549).

Table 1. IC_{50} values and 1st and 2nd electrochemical reduction potentials.

Complex*	IC_{50}, μM A2780	IC_{50}, μM A549	E_{red}, V
1 (1-Cl)	4 (>100)	3 (>100)	−0.40, −1.00
4 (4-Cl)	3 (44)	2 (49)	−0.36
Azpy-NMe_2	>100	14	−1.28
2 (2-Cl)	4 (58)	4 (>100)	−0.33, −0.77
5 (5-Cl)	5 (18)	6 (56)	−0.26, −0.72
Azpy-OH	>100	>100	nd[†]
3 (3-Cl)	>100 (>100)	>100 (>100)	−0.22, −0.74
6 (6-Cl)	39 (>100)	51 (>100)	−0.18, −0.67
Azpy	>100	>100	−1.31 (vs.SCE)[‡]

*Iodido complexes **1**–**6** (and their chlorido analogues **1-Cl** to **6-Cl** in parentheses).
[†]nd, not determined.
[‡]Ref. 14.

4.3. Stability under Physiological Conditions

*For complexes **1**, **2**, **4**, and **5**, no spectral changes (aquation) took place (Figure 3. ^{1}H NMR, ESI-MS).
*For complexes **3**, and **6**, decomposition was observed (Figure 3. ^{1}H NMR, UV-Vis).
*Even in the presence of 104 mM NaCl (close to extracellular [Cl^-]), no change (I to Cl) was observed for the complex **4**.
*Weak cytotoxicity of **3** and **6** would be due to their instabilities in phsphate buffer solution.

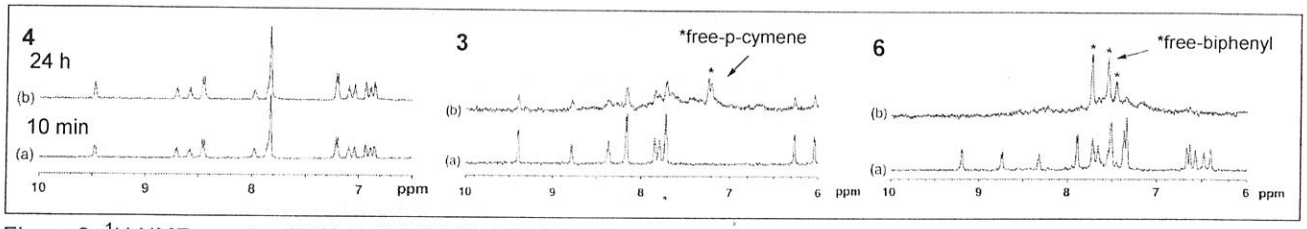

Figure 3. ^{1}H NMR spectra (95% D_2O / 5% MeOD, 10 mM phosphate buffer, pH = 7.3, 37 °C, 24 h)

Which is the stability of [(η^6-arene)Ru(azpy-R)I]PF_6 complexes attributed to azpy-R or I ?

*Corresponding chlorido azpy complexes are also less stabile in water, and showed less cytotoxicity.
(*ex.* [(η^6-biphenyl)Ru(azpy-NMe_2)Cl]PF_6: 24% intact after 24 h)

ref. Sadler, P. J. et al. *Inorg. Chem.* **2006**, 10882.

⇩

The stability of [(η^6-arene)Ru(azpy-R)I]PF_6 complexe is attributed to I.

Remarks: Explanation of less cytotoxicity of corresponding chlorido complex.

[(η^6-biphenyl)Ru(azpy-NMe_2)Cl]PF_6 ⟶ [(η^6-biphenyl)Ru(azpy-NMe_2)(OH_2)]Cl(PF_6)
active to bind to DNA

↓ loss of arene

↓↑

[(η^6-biphenyl)Ru(azpy-NMe_2)(OH)]PF_6
inactive to bind to DNA

Electronegative Cl lowered electron density of Ru center,
which hampers back donation from Ru center to arene ligand leading to loss of arene.

Weak σ-donating & strong π-accepting ligand, azpy, lowered the pK_a value of coordinated H_2O (compare with corresponding en complex).
Thus, not aqua but hydroxo form is predominant under physiological conditions.
Hydroxo complex is relatively inactive to bind to DNA, which leads to less cytotoxicity of chlorido azpy complexes.

ref. Sadler, P. J. et al. *Inorg. Chem.* **2006**, 10882.

4.4. Electrochemical Reductions

*Basically, complexes showed two electrochemical reductions (Table 1, page 8).
First recuction was assigned to addition of an electron into the π orbital centered on the azo group of azpy ligand to form the azo anion radical (-N=N- + e^- ⟶ {-N-N-}$^{\cdot-}$) based on literature assignment.
*Relative order reflects the dcreasing π-acceptor capability of the substituted azpy ligands with the addition of electron-donating groups onto the phenyl ring.

*Second reduction step is assigned to conversion to the dianionic species ({-N-N-}$^{2-}$) based on literature precedents.

*The coordination of azpy ligands to arene-ruthenium centers shifts their reduction potentials to biologically accessible values.

Table 2. Bio-relevant reduction potentials

entry	oxidant	reductant	E_0 (V)	$\Delta G°$ (kcal/mol)
1	succinic acid + CO_2	2-oxoglutaric acid	−0.67	+ 30.9
2	NAD^+	NADH + H^+	−0.32	+ 14.8
3	glutathione (oxidized form)	glutathione (reduced form)	−0.23	+ 10.6
4	pyruvic acid	lactic acid	−0.19	+ 8.7

ref. MOLECULAR CELL BIOLOGY 4th Edition

4.5. Reactions with Glutathione

*Glutathione (GSH) is a tripeptide and a thiol present at millimolar concentrations in cells.

*Complex **4** & corresponding chlorido complex were reacted with GSH (Figure 4, 5).
*Complete substituion of halide by GS^- was observed (HPLC, ESI-MS, Figure 4).
*Iodide substitution occurs 14 times more slowly than chloride substitution.

*Formation of GSSG from GSH was observed by ^1H NMR and ESI-MS (Figure 5).
(LC-MS attempts to detect intermediates were unsuccessful.)

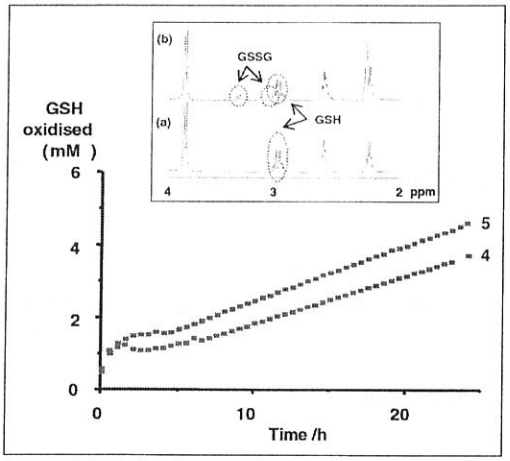

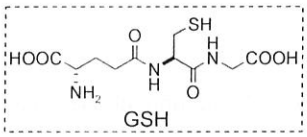

Figure 5. Oxidation of GSH to GSSG observed by ^1H NMR.
10 mM GSH, 100 μM complex, 10 mM phosphate, pH 7.2
85% H_2O / 10% D_2O / 5% acetone-d_6, 37 °C

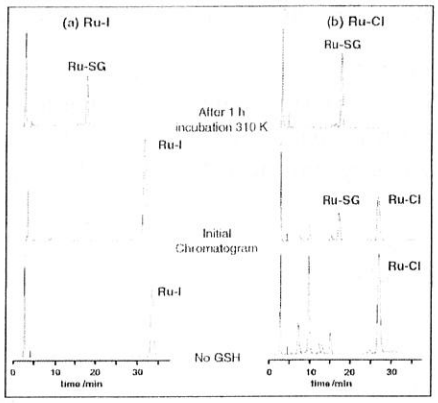

Figure 4. HPLC chromatograms for the reaction of **4** and corresponding chlorido complex
(5 mM GSH, 50 μM complex,)

Other observations

*Bubbles formed in the reaction tubes.
*A variety of methods to detect H_2 were attempted, but none of these led to H_2 detection.
*Small amount of O_2 was detected in the head space of reactions by GC.
*No H_2O_2 was detected by peroxide test sticks.

*Free azpy didn't cause any oxidation of GSH to GSSG.

4.6. Detection of Reactive Oxygen Species (ROS) in A549 Cancer Cells

*Reactive oxygen species: $O_2^{\cdot-}$, $HO_2^{\cdot}$, $HO^{\cdot}$, H_2O_2, and $^1O_2$
*Reactive oxygen species in A549 cell was measured using DCFH-DA (see below).
*DCFH-DA: 2',7'-dichlorodihydrofluorescein-diacetate
This probe measures general oxidative stress.

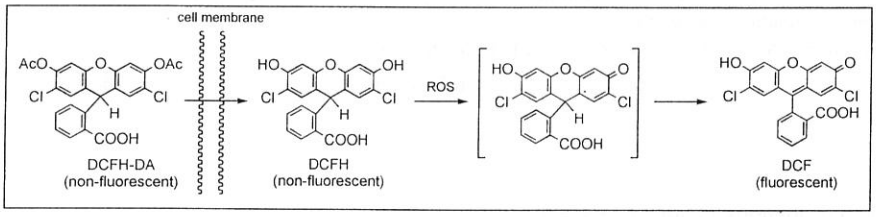

ref. LeBel, C. P. et al. *Chem. Res. Toxicol.* **1992**, *5*, 227.

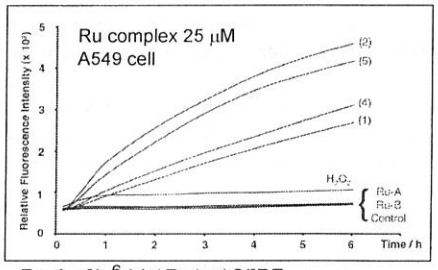

Ru-A : $[(\eta^6\text{-bip})Ru(en)Cl]PF_6$
Ru-B : $([\eta^6\text{-tha})Ru(en)Cl]PF_6$
bip : biphenyl, tha : tetrahydroanthracene

Figure 6. Relative increase in DCF fluorescence.

*Complexes **1**, **2**, **4**, and **5** increase the level of ROS inside A549 cells (Figure 6).
*Control complexes Ru-A and Ru-B caused no increase in the level of ROS.

*A549 cell pretreated with *N*-acetyl-L-cysteine (NAC), which is known to increase thiol levels in cell was examined in a cell survival assay (Figure 7).
*There is greater cell survival for the cells that have increased thiol levels.

These data provide the evidence that ROS are implicated in cell death.

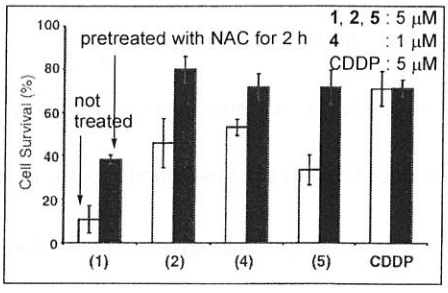

NAC : *N*-acetyl-L-cysteine, CDDP : cisplatin

Figure 7. Cell survival after 24 h using A549 cell pretreated with 5 mM NAC.

4.7. Proposed Mechanism and Consideration

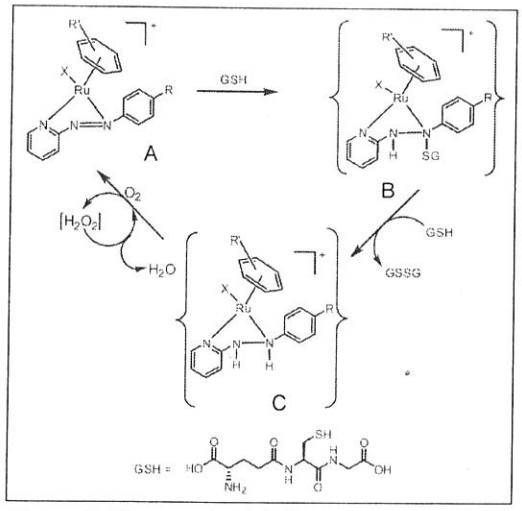

Figure 8. Proposed catalytic cycle.

*X is at first iodide, then is displaced by GS^- during the early stages.
*Activated azo functionality by cationic ruthenium center (Figure 8).
*Similar reaction to conversion of azo group to hydrazine group by glutathione has been reported although it is a stoichiometric reaction.
ex. J. Med. Chem. **1972**, *15*, 307.

*C is oxidized by dissolved O_2 to generate H_2O_2 and catalyst.
*Given that no H_2O_2 was detected, it would be reduced to H_2O to generate O_2, which might be catalyzed by iodide displaced from Ru.

$$I^- + H_2O_2 \longrightarrow IO^- + H_2O$$
$$IO^- + H_2O_2 \longrightarrow I^- + H_2O + O_2$$

ref. Hansen, J. C.
J. Chem. Educ. **1996**, *73*, 728.

*Ruhenium arene complexes containing ethylenediamine (en) as chelating ligand, which are also anticancer agents, showed no ROS generation, indicating a fundamental difference in the mechanism of action (Figure 6).

*Because GSH is the primary cellular antioxidant, depletion of antioxidants caused by the Ru-complex leads to increase of ROS level.
*Cancer cells are known to be more sensitive to ROS than normal cells, meaning that the complexes studied here could be used to treat cancer.

For sensitivity of cancer cell to ROS, see: Agostinelli, E. and Seiler, N. *Amino Acids* **2006**, *31*, 341.

4.8. Outlook

*Deep knowledge about effects of ligands on the bioactivity of complexes.
*Selectivity between cancer cells and normal cells